Response of Subpolar North Atlantic Meridional Overturning Circulation to Variability in Surface Winds on Different Timescales

MARGARITA Y. MARKINA,[a] HELEN L. JOHNSON,[a] AND DAVID P. MARSHALL[b]

[a] *Department of Earth Sciences, University of Oxford, Oxford, United Kingdom*
[b] *Department of Physics, University of Oxford, Oxford, United Kingdom*

(Manuscript received 20 November 2023, in final form 28 May 2024, accepted 6 June 2024)

ABSTRACT: A large part of the variability in the Atlantic meridional overturning circulation (AMOC) and thus uncertainty in its estimates on interannual time scales comes from atmospheric synoptic eddies and mesoscale processes. In this study, a suite of experiments with a 1/12° regional configuration of the MITgcm is performed where low-pass filtering is applied to surface wind forcing to investigate the impact of subsynoptic (<2 days) and synoptic (2–10 days) atmospheric processes on the ocean circulation. Changes in the wind magnitude and hence the wind energy input in the region have a significant effect on the strength of the overturning; once this is accounted for, the magnitude of the overturning in all sensitivity experiments is very similar to that of the control run. Synoptic and subsynoptic variability in atmospheric winds reduce the surface heat loss in the Labrador Sea, resulting in anomalous advection of warm and salty waters into the Irminger Sea and lower upper-ocean densities in the eastern subpolar North Atlantic. Other effects of high-frequency variability in surface winds on the AMOC are associated with changes in Ekman convergence in the midlatitudes. Synoptic and subsynoptic winds also impact the strength of the boundary currents and density structure in the subpolar North Atlantic. In the Labrador Sea, the overturning strength is more sensitive to the changes in density structure, whereas in the eastern subpolar North Atlantic, the role of density is comparable to that of the strength of the East Greenland Current.

SIGNIFICANCE STATEMENT: A key issue in understanding how well the Atlantic meridional overturning circulation is simulated in climate models is determining the impact of synoptic (2–10 days) and subsynoptic (shorter) wind variability on ocean circulation. We find that the greatest impact of wind changes on the strength of the overturning is through changes in energy input from winds to the ocean. Variations in winds have a more modest impact via changes in heat loss over the Labrador Sea, alongside changes in wind-driven surface currents. This study highlights the importance of accurately representing the density in the Labrador Sea, and both the strength and density structure of the East Greenland Current, for the correct representation of overturning circulation in climate models.

KEYWORDS: Synoptic-scale processes; Thermohaline circulation; Wind; Ocean models; Oceanic variability

1. Introduction

The Atlantic meridional overturning circulation (AMOC) plays a crucial role in the climate system by facilitating poleward heat transport in the ocean and is projected to weaken in the future as a result of anthropogenic greenhouse gas emissions (IPCC 2021). However, the variability of the AMOC on decadal and longer time scales is often obscured by large interannual and seasonal fluctuations (Moat et al. 2020; Jackson et al. 2022). Recent observations have revealed significant interannual variability in the AMOC at subpolar latitudes (Lozier et al. 2019; Li et al. 2021) with both wind and buoyancy forcing considered to be important drivers on these time scales (Biastoch et al. 2008; Yeager and Danabasoglu 2014; Larson et al. 2020; Kostov et al. 2021).

A large part of AMOC variability and thus uncertainty in its estimates on interannual time scales comes from atmospheric synoptic eddies and mesoscale processes (Buckley and Marshall 2016; Sinha et al. 2013). It is generally accepted that the major influence of wind stress on AMOC anomalies comes from Ekman transports and wind-induced geostrophic currents (Jackson et al. 2022). On interannual time scales, westward propagating Rossby waves generated by fluctuations in wind stress curl are known to have an important effect on AMOC variability (e.g., Barnier 1988; Sinha et al. 2013). Wind speed is intricately linked to surface buoyancy fluxes, affecting magnitudes of sensible and latent heat fluxes as well as modifying the freshwater fluxes through evaporation. The strength and the anomaly of wind stress curl is important for the strength and the position of the subpolar gyre and defines the position of the North Atlantic Current, impacting salinity in the eastern part of the basin (Holliday et al. 2020); the latter is important for surface water mass transformations and the AMOC.

The extant literature has explored the AMOC response to the magnitude of winds and generally shows a slowdown of AMOC when the magnitude of wind stress is reduced (Lohmann et al. 2021; Putrasahan et al. 2019; Yang et al. 2016). A number of studies have explored the response of the AMOC to wind stress anomalies associated with the North Atlantic Oscillation (NAO), which is the dominant mode of atmospheric variability in the North Atlantic sector (e.g., Visbeck et al. 1998; Delworth and

Denotes content that is immediately available upon publication as open access.

Corresponding author: Margarita Markina, margarita.markina@earth.ox.ac.uk

DOI: 10.1175/JPO-D-23-0236.1

Greatbatch 2000; Marshall et al. 2001; Eden and Jung 2001; Sarafanov 2009). The AMOC shows a lagged oceanic response to atmospheric variability (Xu et al. 2013; Danabasoglu et al. 2016; Böning et al. 2006) and seems to be more sensitive to the positive phase of NAO (e.g., Lohmann et al. 2009). Other studies (e.g., Eden and Willebrand 2001; Deshayes and Frankignoul 2008; Khatri et al. 2022) have demonstrated a fast barotropic oceanic response to wind stress anomalies associated with the NAO on intraseasonal time scales that is coming from the Ekman transports and a delayed baroclinic oceanic response on the scale of several years connected to the spin up of the subpolar gyre.

However, the effects of wind variability across different temporal scales on the AMOC have yet to be fully elucidated. Such considerations are particularly germane given the limited spatial resolution of the phase 6 of Coupled Model Intercomparison Project (CMIP6) models, which may not fully capture the dynamics of intense cyclonic events and mesoscale processes in the atmosphere. In the North Atlantic sector, atmospheric cyclones do not propagate poleward enough in coupled climate model simulations (Priestley et al. 2023). Furthermore, the spatial resolution of the climate models is not always sufficient to resolve the frequency of high-intensity cyclones (Priestley et al. 2020) as well as mesoscale processes in the atmosphere such as tip jets, katabatic winds, and cold-air outbreaks that are also associated with strong air–sea heat fluxes (Våge et al. 2009; Condron and Renfrew 2013; Moore 2014; Papritz and Spengler 2017; Josey et al. 2019; Gutjahr et al. 2022) and play an important role for surface water mass transformation and thus overturning at subpolar latitudes. In this way, understanding the differential effect of atmospheric flow decomposed into different length and time scales on the AMOC can contribute a new perspective in understanding projections of meridional overturning circulation (MOC) in the future.

This study investigates the effects of winds across different temporal scales on the AMOC, with a particular focus on synoptic and higher-frequency variability. Using a suite of sensitivity experiments with a 1/12° regional configuration of the MITgcm, we apply low-pass filtering to surface winds to extract variability associated with mesoscale processes and atmospheric cyclones and examine the impact of wind magnitude and variability on the circulation in the subpolar North Atlantic. Our experimental approach is described in section 2, where we also provide a brief rationale for our methods. In sections 3–5, we present our main findings on the influence of wind on the properties of the upper ocean, meridional transports of heat and salt, and the overturning circulation. Finally, in section 6, we summarize and discuss our results.

2. Model setup and experiment design

We conduct numerical experiments using the MITgcm ocean general circulation model (Adcroft et al. 2018; Marshall et al. 1997) coupled with a dynamic–thermodynamic sea ice model (Losch et al. 2010; Heimbach et al. 2010). The model solves the primitive equations in rescaled z^* coordinates (Adcroft and Campin 2004). The model is run on a latitude–longitude–cap grid; its computational domain covers the North Atlantic region from ~10°S to ~73°N which permits us to include the equatorial

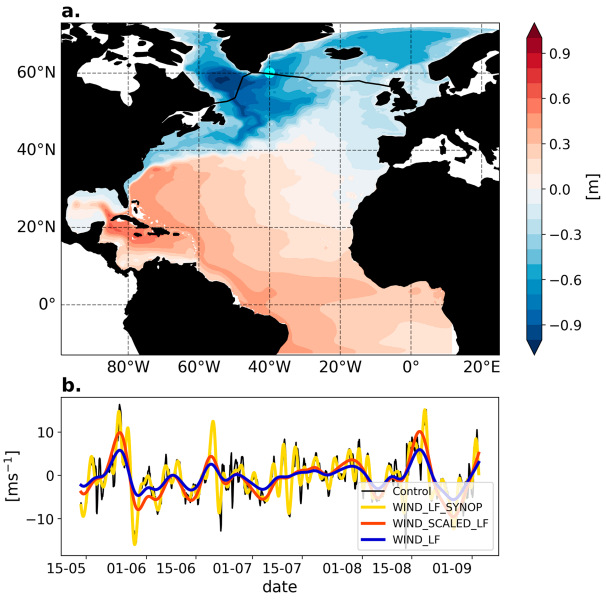

FIG. 1. (a) Mean relative dynamic sea surface height during the winter season (January–March) of years 11–15 over the regional domain of the MITgcm; (b) 4 months' time series of 10-m zonal wind speed in the location shown with the cyan dot in (a) in the Irminger Sea. The time series comprises JRA55-do reanalysis data used as forcing for the control experiment (black), along with filtered low-frequency winds (blue), low-frequency plus synoptic winds (yellow), and scaled low-frequency winds (red) used as wind forcing in three sensitivity experiments. The black line in (a) shows the position of the observational OSNAP array.

waveguide, while remaining computationally efficient (Fig. 1a). The model is eddy rich with a nominal horizontal resolution of 1/12° and 50 vertical levels. The integration time step is 5 min, and we use the seventh-order advection scheme. We prescribe lateral open boundary conditions from the Arctic Subpolar State Estimate (ASTE) (Nguyen et al. 2021), based on an ocean–sea ice model constrained by a large amount of satellite and in situ observations. Meridional velocities at the southern boundary of the domain are adjusted to ensure that the volume budget is closed. A sponge layer for velocity fields is applied at the lateral boundaries, with a thickness of 24 grid cells (2°). The model is forced by time-varying repeated year forcing from JRA-55 dataset for driving ocean–sea models (JRA55-do) (Tsujino et al. 2018) corresponding to 1 May 2003–1 May 2004, following Stewart et al. (2020). This period is chosen since it is neutral in terms of the NAO phase, and the transition day at the beginning of May avoids large high-latitude variability in forcing fields and deep water formation that takes place in winter and early spring. The model is initialized with temperature and salinity fields from World Ocean Atlas corresponding to May 2003. After initialization, the model is spun up into a statistically steady state by running it for 50 years. All simulations (including the control run) are then run for 15 repeated years starting from the end of this 50-yr model spinup.

The control run demonstrates a reasonable representation of the oceanic circulation in the region. Subtropical and subpolar

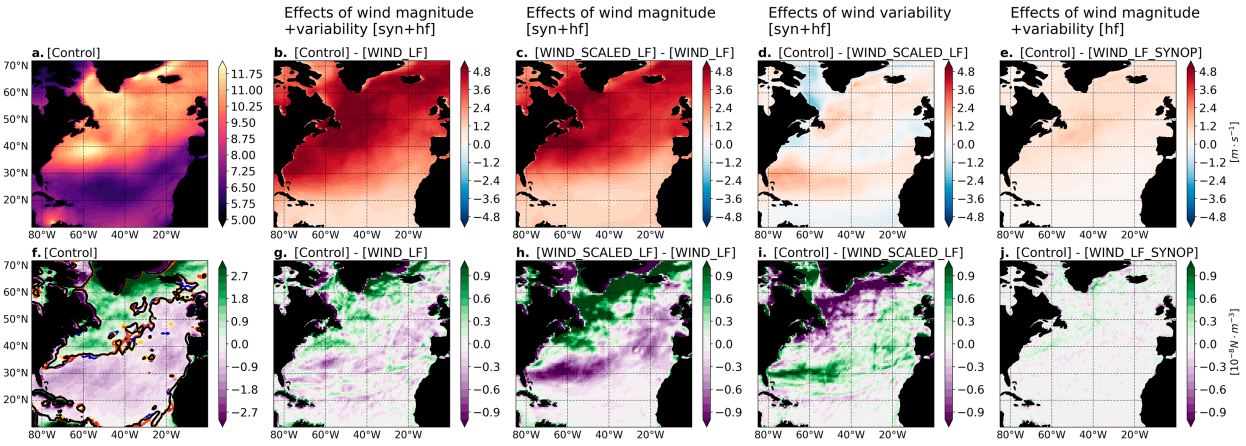

FIG. 2. (a) Wind speed and (f) wind stress curl in JRA55-do averaged over the period from 1 May 2003–1 May 2004 (corresponding to repeated year forcing period), colored contours in (e) show zero curl line in control experiment (black), experiment forced by low-frequency winds (blue), low-frequency plus synoptic winds (yellow), and scaled low-frequency winds (red). (b),(g) The differences between control and low-frequency winds. (c),(h) The differences between scaled and nonscaled low-frequency winds. (d),(i) The differences between control and scaled low-frequency winds. (e),(j) The differences between control and low-frequency plus synoptic winds.

gyres are clearly identifiable (Fig. 1a), with the Gulf Stream appropriately separating from the North American coast near Cape Hatteras (Fig. 1a). The strength of the basinwide AMOC in depth space reaches up to 21 Sv (1 Sv $\equiv 10^6$ m^3 s^{-1}) which is within the range of the estimates in global eddy-rich models (Hirschi et al. 2020). Furthermore, the model accurately positions the sea ice edge (Fig. 3f). However, it is important to note that our model exhibits a salinity bias when compared to the Overturning in the Subpolar North Atlantic Program (OSNAP) observations in the subpolar North Atlantic (Lozier et al. 2019; Li et al. 2021). The mean salinity across the OSNAP line (position shown in Fig. 1a) in our control run is approximately 0.5 psu higher than the observed values of salinity. Specifically, our model forced by repeated year forcing corresponding to May 2003–04 yields a mean salinity of 35.40 psu along the OSNAP line, while the observations (during May 2014–August 2018) indicate a salinity of 34.92 psu (Lozier et al. 2019). The gradient of salinity across the OSNAP East section (estimated as the difference between mean values shallower than 500 m in the western and eastern parts of the OSNAP East line) is larger in the control run compared to the observations (1.09 vs 0.99 psu), while the temperature gradient is lower in the model; this leads to a lower density gradient in the upper 500 m in the control run compared to the observations (0.08 vs 0.14 kg·m^{-3}). Salinity bias in the Labrador Sea in models may lead to a greater influence of temperature on density on decadal and interannual time scales (Menary et al. 2015). Acknowledging this limitation, we also note that the overestimation of salinity in this region is a common feature in eddy rich models and is due to a stronger subpolar gyre (Hirschi et al. 2020; Petit et al. 2023).

To investigate the sensitivity of the AMOC to synoptic and higher-frequency variability in atmospheric winds, we perform a suite of sensitivity experiments by applying low-pass filtering to atmospheric winds and forcing the ocean model with these filtered winds. Throughout this manuscript, we refer to the experiment forced by the original JRA55-do winds as the control experiment, which serves as the reference model run. Later, we decompose the wind forcing into three components corresponding to short-term subsynoptic variability (0–2 days), synoptic-scale variability (defined here as 2–10 days; e.g., Hoskins and Hodges 2002), and low-frequency variability (more than 10 days) using a bandpass Lanczos filter (Lanczos 1956; Duchon 1979) as in a number of studies (Ayrault et al. 1995; Gulev et al. 2002; Foussard et al. 2019; Markina et al. 2019). Filtering the wind yields two distinct effects: the modulation of temporal variability and the alteration of magnitude. As an example, a 4-month long time series of 10-m zonal winds in the four experiments performed in this study is shown in Fig. 1b.

Throughout the manuscript, we use the notation WIND_LF_SYNOP to refer to the experiment where we filter out variability of surface winds on periods shorter than 2 days (i.e., the difference between the control run and WIND_LF_SYNOP allows us to see the impact of small cyclones and mesoscale variability) and WIND_LF to refer to the experiment where we exclude synoptic plus higher-frequency atmospheric variability from the forcing winds, leaving only the impact of low-frequency atmospheric variability on time scales larger than 10 days. In this way, the difference between the control and WIND_LF experiments allows us to see the impact of synoptic and higher-frequency processes in the atmosphere.

Figure 2 (upper panel) shows the mean wind speed from JRA55-do that is used to force the control run from 1 May 2003 to 1 May 2004, as well as the differences in wind speed between the control run and experiments forced by filtered winds. When we apply a filter to remove both synoptic and higher-frequency variability (WIND_LF experiment; Fig. 2b), the wind speed magnitude decreases compared to the control run, with differences of up to 5 m s^{-1} observed in subpolar latitudes. This suggests that a combination of synoptic and higher-frequency winds contributes significantly to the input of wind energy. In contrast, subsynoptic winds (with periods

shorter than 2 days) have a much lesser impact on the wind energy input.

Due to the filtering procedure, the low-frequency winds in our experiment have lower magnitude than in the control experiment (Fig. 1b, blue vs black line). To explore the impact of variability in atmospheric winds on oceanic circulation, while accounting for differences in magnitude, we conduct an additional experiment denoted WIND_SCALED_LF. In this experiment, we scale the low-frequency winds such that the total energy input ($\mathbf{U}^2$) over time in each grid cell remains consistent with the control run (Fig. 1b). In this way, in the WIND_SCALED_LF experiment, the synoptic and subsynoptic atmospheric eddies are filtered out, and the winds are smoother compared to the control run (Fig. 1b, red vs black line), which leads to large-scale wind patterns persisting for longer periods without being effectively damped. The magnitude of the wind speed does not change significantly, with differences of up to 2 m s^{-1} compared to the control run (Fig. 2d). This difference is comparable to the influence of subsynoptic and mesoscale processes seen in Fig. 2e.

In subsequent analyses presented in this paper, plots with five columns follow a consistent format. The first column displays the mean values derived from the control run. The second column illustrates the influence of synoptic and higher-frequency winds (capturing *both magnitude and variability*), the third column separately captures the effect of *magnitude* in synoptic and higher-frequency winds, and the fourth column separately captures the effect of *variability* in synoptic and higher-frequency winds. Finally, the fifth column isolates the impact of higher-frequency winds alone (both their magnitude and variability). Plots with only four columns show the effects of winds described above that have been averaged over 5-yr periods, without showcasing the mean values obtained from the control run. We note that comparing WIND_SCALED_LF and WIND_LF (which differ only in magnitude) reveals very similar patterns to those observed when comparing the control and WIND_LF experiments. This suggests that the differences between the control and WIND_LF runs are primarily due to wind magnitude rather than wind variability.

3. Effects of low-pass wind filtering on wind stress curl and Ekman transport

In section 1, we discussed how changes in wind stress curl and Ekman transport can impact ocean circulation. The lower section of Fig. 2 shows the wind stress curl averaged over a repeated year forcing period (1 May 2003–1 May 2004), as well as the differences between control and sensitivity experiments. The zero wind stress curl line, which runs from the North American coast to Scotland, remains in the same position in all experiments (Fig. 2f, shown in contours). This suggests that we may not see changes in the position of the North Atlantic Current related to shifts in the zero curl line.

Synoptic and higher-frequency winds (<10 days) that are present in the control and not in the WIND_LF experiment contribute to a larger wind stress curl in the subpolar regions and lower curl in the subtropics (Fig. 2g), similar to the positive NAO phase (e.g., Barrier et al. 2014). The weakened circulation pattern in the WIND_LF experiment corresponds to a reduction in Ekman transport in the tropics and midlatitudes, resulting in weaker convergence between 26° and 50°N compared to the control experiment as shown in Table 1. In contrast, when comparing the control run with the WIND_SCALED_LF experiment (Fig. 2i), there is a negative wind stress curl anomaly in subpolar latitudes and a positive anomaly in the subtropics, similar to the negative NAO phase (e.g., Barrier et al. 2014). As we mentioned in section 2, in the WIND_SCALED_LF run, the atmospheric winds exhibit a smoother behavior compared to the control run (Fig. 1b) and large-scale wind patterns persist for longer periods. As a consequence, there is an amplification of the wind stress curl, particularly in regions naturally characterized by strong wind stress curl, such as the subpolar and subtropical latitudes.

TABLE 1. Ekman transport at 26° and 50°N in each experiment averaged over the repeated year forcing period (May 2003–04).

Experiment	Ekman transport at 26°N (Sv)	Ekman transport at 50°N (Sv)
Control	0.43	−0.17
WIND_LF	0.40	−0.14
WIND_LF_SYNOP	0.43	−0.17
WIND_SCALED_LF	0.54	−0.26

4. Surface and upper-ocean properties

During the winter season, the ocean in mid- and subpolar latitudes experiences heat loss to the atmosphere (Fig. 3a). This heat loss is amplified by stronger surface winds, associated with synoptic and subsynoptic atmospheric processes (Fig. 3c) with the largest anomaly observed in the Labrador Sea. This highlights the importance of these atmospheric processes for the heat loss in this region. The amplification occurs through changes in sensible and latent heat fluxes, introduced into the model's bulk formulas by the winds. This larger heat loss leads to a deeper mixed layer in the Labrador Sea (Fig. 3h). While the mean mixed layer depth (MLD) in March in our control experiment (Fig. 3f) aligns well with observations (Holte et al. 2017), maximal values of mixed layer depth in winter can reach the bottom of the Labrador Sea in some individual years (not shown) due to higher salinity in our model compared to observations. Contours in Fig. 3f also shows 15% sea ice concentration in all simulations and demonstrate that the experiments do not exhibit substantial changes of the sea ice edge.

The larger magnitudes and variability of surface winds have a cooling effect on the upper-ocean waters throughout the subpolar gyre (Figs. 4a,e,i). This cooling is particularly prominent in the Irminger Sea and along the boundary currents during the first 5 years of the experiment (Fig. 4a). After this initial period, the advection of warm and salty subtropical waters into the subpolar North Atlantic becomes evident (Figs. 4e,i and 5e,i). The experiment, forced by surface winds with larger magnitude, initially exhibits more saline waters in the central

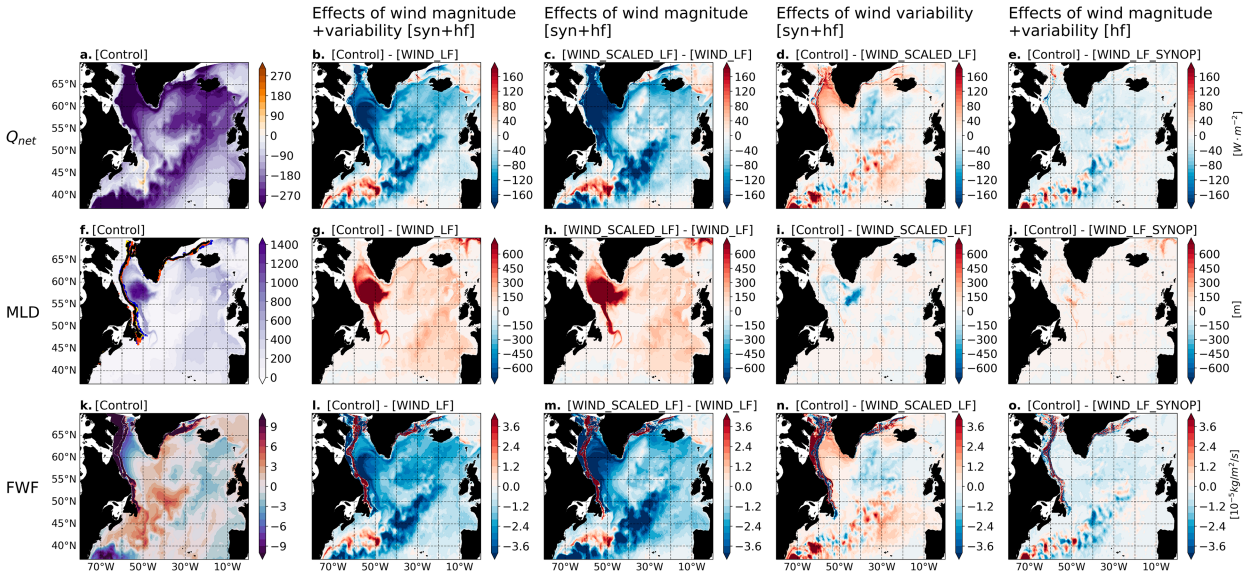

FIG. 3. (a) Net heat flux into the ocean (Q_{net}) in winter (January–March), (f) mean MLD in March, and (k) freshwater flux into the ocean in winter (January–March) in years 11–15 in control experiment. Negative values of net heat flux correspond to the ocean losing heat to the atmosphere; positive values of freshwater flux correspond to decrease in salinity. Colored contours in (f) show 15% concentration of the sea ice in control experiment (black), experiment forced by low-frequency winds (blue), low-frequency plus synoptic winds (yellow), and scaled low-frequency winds (red). (b),(g),(l) The differences between control and experiment forced by low-frequency winds (highlighting the effect of wind magnitude and variability associated with synoptic and higher-frequency winds). (c),(h),(m) The differences between the experiments forced by scaled vs nonscaled low-frequency winds (highlighting the effect of wind magnitude associated with synoptic and higher-frequency winds). (d),(i),(n) The differences between control and experiment forced by scaled low-frequency winds (highlighting the effect of wind variability associated with synoptic and higher-frequency winds). (e),(j),(o) The differences between control and experiment forced by low-frequency and synoptic winds (highlighting the effect of wind magnitude and variability associated with synoptic and higher-frequency winds).

Labrador Sea (Fig. 5b) possibly due to deeper convection and mixed layers which entrain salty water from below. After 5 years, the advection of saltier subtropical waters also becomes apparent, and after 10 years, it spreads across the entire basin, including the boundary current in the Labrador Sea, with the Irminger Sea exhibiting the most substantial differences between the control run and WIND_LF experiment.

The subsynoptic variability of surface winds has a relatively uniform impact over the basin: it contributes to marginally more intense heat loss (Fig. 3e), deeper mixed layers (Fig. 3j), and reduced freshwater input into the ocean (Fig. 3o). Over the years, subsynoptic winds lead to the development of denser upper-ocean waters in the western subpolar North Atlantic and somewhat lighter waters in the eastern subpolar North Atlantic (Figs. 6d,h,l). The warmer and more saline waters in the eastern subpolar North Atlantic appear to be originating from the tropics, indicating that the lighter densities are associated with warmer temperatures (Figs. 4–6d,h,l). This is supported by the fact that the light-density anomalies transition to dense anomalies before reaching the Greenland–Scotland Ridge.

The control experiment, which includes synoptic and high-frequency atmospheric variability, exhibits reduced heat loss from the ocean to the atmosphere in the Labrador Sea compared to the WIND_SCALED_LF experiment where this variability is filtered out (Fig. 3d). This could reflect the role of the more persistent atmospheric patterns in the WIND_SCALED_LF experiment in enhancing the heat loss in the Labrador Sea and is also consistent with moderately larger wind speed in the western subpolar North Atlantic in wintertime (Fig. 2d) in that experiment. This reduced heat loss in the Labrador Sea in the control experiment precedes the higher temperatures and enhanced heat loss in the Irminger Sea (not shown). A number of studies using Lagrangian particle tracking have shown that the time scales for fast propagation of density anomalies in the upper layer from the Labrador into the Irminger Sea are from a few months to about 2 years (Chafik et al. 2022; Fox et al. 2022; Furey et al. 2023), consistent with our estimates. In this way, we suggest that as a result of different heat loss in the Labrador Sea, there is an advection of warmer and saltier waters from the Labrador Sea interior into the Irminger Sea interior (third columns in Figs. 4 and 5) that in turn leads to the enhanced heat loss and reduction in the freshwater flux in eastern subpolar North Atlantic seen in years 11–15 in Figs. 3d and 3n.

Comparing the control and WIND_SCALED_LF experiment, temperature seems to have a dominant effect on the change in density in the eastern subpolar gyre (third column in Figs. 4–6). This contrasts with the WIND_LF experiment, where density anomalies in the eastern subpolar North Atlantic are dominated by the effect of salinity (Figs. 4–6i). We

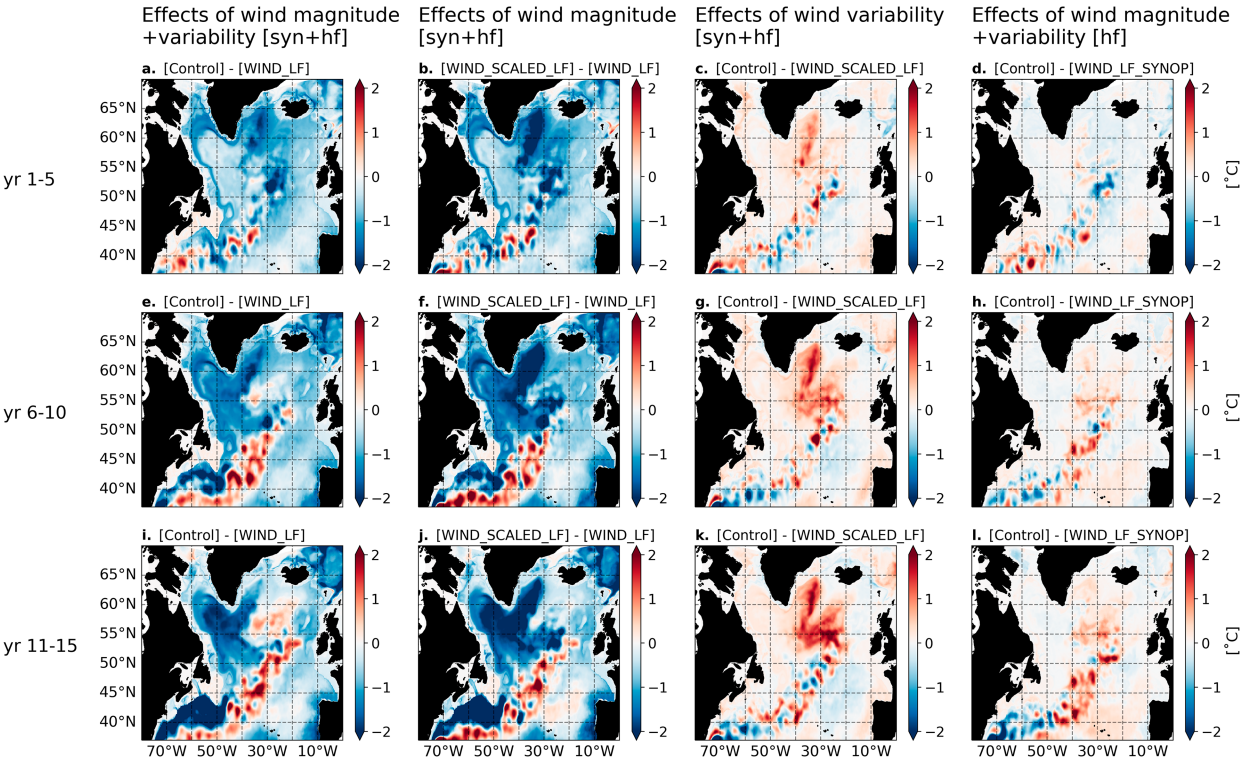

FIG. 4. Differences in mean potential temperature in the upper 500 m between the control run and sensitivity tests, averaged over (a)–(d) years 1–5, (e)–(h) years 6–10, and (i)–(l) years 11–15. (a),(e),(i) The differences between control and experiment forced by low-frequency winds (highlighting the effect of wind magnitude and variability associated with synoptic and higher-frequency winds). (b),(f),(j) The differences between the experiment forced by scaled versus nonscaled low-frequency winds (highlighting the effect of wind magnitude associated with synoptic and higher-frequency winds). (c),(g),(k) The differences between control and experiment forced by scaled low-frequency winds (highlighting the effect of wind variability associated with synoptic and higher-frequency winds). (d),(h),(l) The differences between control and experiment forced by low-frequency and synoptic winds (highlighting the effect of wind magnitude and variability associated with synoptic and higher-frequency winds).

suggest that this difference is due to the origin and persistence of the temperature anomalies. Specifically, when these anomalies come from subpolar latitudes (WIND_SCALED_LF), they tend to remain and significantly contribute to the densification process. Conversely, when anomalies that are both warmer and saltier emerge from tropical regions (WIND_LF), they rapidly cool down. This rapid loss of heat elevates the impact of salinity on density in the eastern subpolar gyre.

The gyres are stronger in the control run compared to the WIND_LF experiment (Fig. 7b) where the magnitude and variability of surface winds are reduced. The comparison between WIND_SCALED_LF and WIND_LF experiments (Fig. 7c) shows that this strengthening of the gyre is due to the magnitude of the surface winds. This explains larger advection of warm and salty subtropical waters into the subpolar North Atlantic shown in Figs. 4 and 5 (panels e, i and also f, j). In the control run, where all modes of atmospheric variability are present, the subpolar gyre is generally weaker compared to the WIND_SCALED_LF experiment, where synoptic and higher-frequency variability are subtracted and large-scale wind patterns are more persistent (Fig. 7d). Note that in Figs. 7b–e, negative anomalies within the subpolar gyre indicate a strengthening of the gyre, while positive anomalies indicate a weakening. This is due to the climatological subpolar gyre being negative (as shown in Fig. 7a), which is indicative of its counterclockwise circulation. In this way, the magnitude of surface winds is important for sustaining the strength of the gyres, while larger synoptic and subsynoptic variability of atmospheric winds lead to the weakening of the subpolar gyre due to the dampening effect of atmospheric eddies. The largest differences in current speed are observed along the boundary currents in the Irminger and Labrador Seas, as well as in the region around the North Atlantic Current where the differences exhibit a more eddying structure (Figs. 7l–o). The separation line between subtropical and subpolar gyres and the position of the North Atlantic Current do not exhibit a noticeable shift in any of the three perturbed wind forcing experiments (Figs. 7a–e).

5. Meridional transports of heat and freshwater and overturning circulation

The magnitude and synoptic and subsynoptic variability of surface winds impact both upper-ocean temperatures and

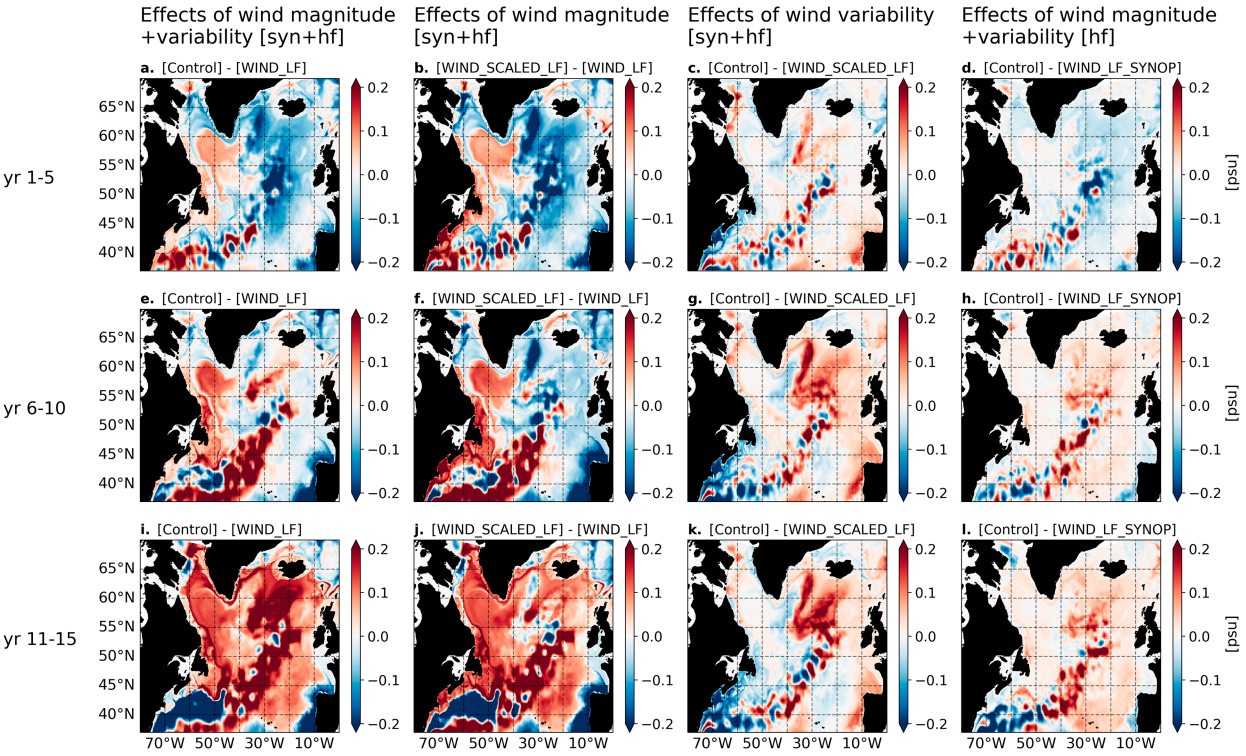

FIG. 5. As in Fig. 4, but for salinity in the upper 500 m.

salinities and lead to variations in the strength of the gyres. Figure 8 illustrates the meridional transports of heat and freshwater across 40°N in the four experiments, calculated following the methodology described in Lozier et al. (2019), with the exception that we use a reference salinity of 35 psu. In the experiment where synoptic and higher-frequency variability of atmospheric winds are filtered out (WIND_LF), there is an initial enhancement of meridional heat and freshwater transport across 40°N (solid lines in Fig. 8). This can be attributed to a reduction in southward Ekman transport in the midlatitudes in these experiments compared to the control run (Table 1). However, following an initial 3–4-yr period, the meridional heat and freshwater transport decrease in both the WIND_LF and WIND_LF_SYNOP, that can be attributed to the weakening of the subpolar gyre (Figs. 7b,e) resulting from the reduction in the magnitude of surface winds. After 15 years, the heat and freshwater transports in WIND_LF stabilize and do not experience further weakening (not shown).

On the other hand, the WIND_SCALED_LF experiment, where synoptic and higher-frequency variability of surface winds are filtered out but energy input is the same as in the control run, is characterized by stronger wind stress curl (Fig. 2i) and increased southward Ekman transport in the midlatitudes (Table 1). During the initial 4 years, the heat transport in the WIND_SCALED_LF experiment is lower compared to the control run (Fig. 8a). This is attributed to the larger southward Ekman transport in the midlatitudes in the WIND_SCALED_LF compared to the control run (Table 1). However, in the subsequent period, the magnitude of heat transport across 40°N aligns more closely with the control run. This is due to the higher temperatures in the eastern subpolar North Atlantic (as shown in the third column of Fig. 4) offsetting the weaker gyre in the control run, resulting in a similar magnitude of heat transport in both the control and WIND_SCALED_LF experiments at this latitude.

Larger magnitude winds lead to a stronger AMOC with a deeper core which is evident when we compare both control and also WIND_SCALED_LF experiments to the WIND_LF experiment (first and second columns in Fig. 9). This is consistent with enhanced convection and deeper mixed layers in the control experiment (Figs. 3g,h) and likely reflects a stronger deep western boundary current (not shown). The subsynoptic variability of atmospheric winds results in a similar pattern of the AMOC change, but with smaller magnitude (Figs. 9d,h,l).

In contrast, synoptic and high-frequency wind variability in the control experiment lead to stronger AMOC in the subpolar latitudes and weaker AMOC in the subtropics (Fig. 9c) compared to the WIND_SCALED_LF run. This pattern is related to smaller downwelling around 40°N in the control run due to reduced Ekman convergence (Table 1). This dipole pattern in the AMOC during the first 5 years (Fig. 9c) is also reminiscent of the transient ocean response to changes in Ekman transport. These changes are typically associated with anomalies in surface wind stress curl during the positive phase of the NAO (e.g., Eden and Willebrand 2001; Martin et al.

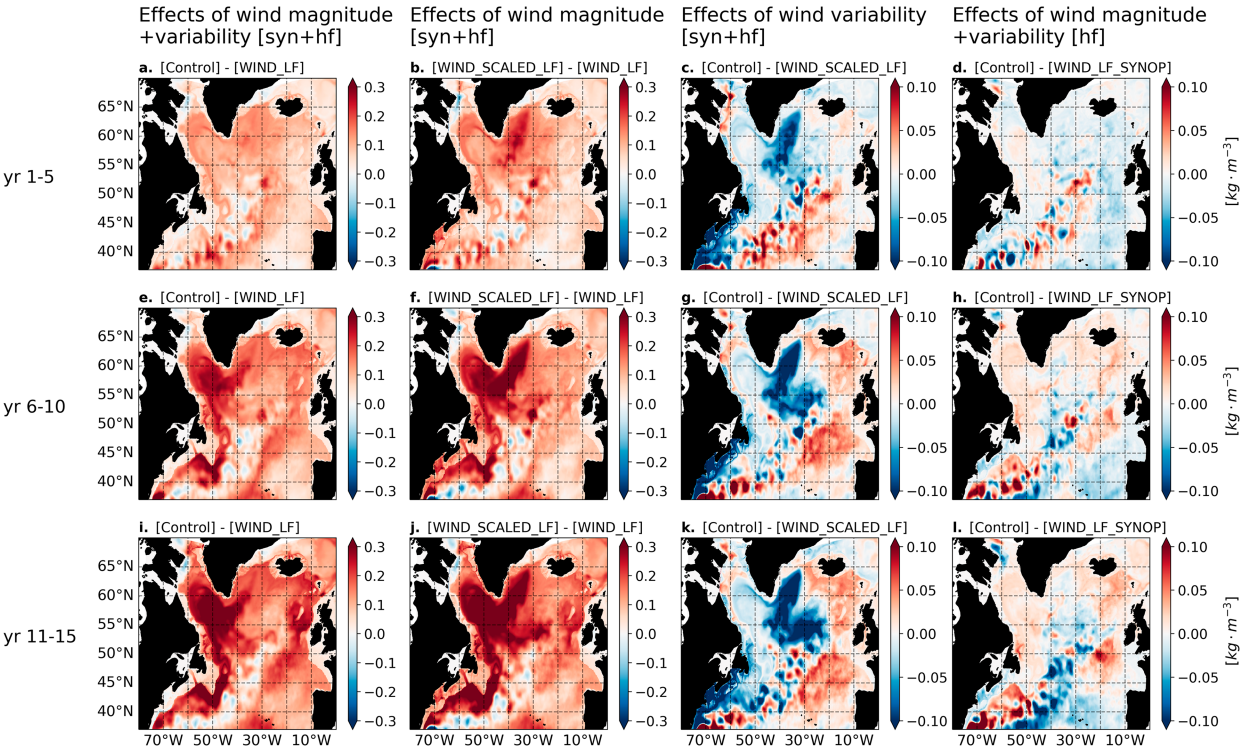

FIG. 6. As in Fig. 4, but for mean potential density (σ_0) in the upper 500 m.

2019; Khatri et al. 2022). In our case, however, this pattern exhibits opposite signs, which is consistent with the wind tress curl being weaker in the control experiment compared to WIND_SCALED_LF as illustrated in Fig. 2i and discussed in section 3. After the first 5 years (Fig. 9g), the negative anomaly in the lower limb propagates southward and also spreads northward up to ~45°N which could be an imprint of weaker subpolar gyre in the control run compared to the WIND_SCALED_LF experiment (Fig. 7d). This is also consistent with the shallowing mixed layers in the subpolar North Atlantic (Fig. 3i) and a weakening of the deep western boundary current (not shown).

The features observed around 36°–39°N in Figs. 9c, 9g, and 9k are consistent with variations in the strength and position of the standing eddy near the Gulf Stream separation point (Figs. 7i,j) that projects onto the overturning streamfunction. It is worth noting that the interaction between eddies and the underlying topography in the Gulf Stream separation region often gives rise to such features in eddy-resolving models (Chassignet and Marshall 2008). The strength of this standing eddy in the control experiment is weaker compared to the WIND_LF_SYNOP experiment (Fig. 9l), and its position exhibits a slight displacement compared to the WIND_SCALED_LF experiment (Figs. 9c,g,k).

To estimate the total volume of lighter water moving northward in the upper limb and denser waters moving southward in the lower limb in the subpolar North Atlantic, we also look at the meridional overturning streamfunction in density space. Figure 10 compares the overturning streamfunction between our model experiments and observations taken along the OSNAP line (Figs. 10a–c) that extends from the Labrador Sea, traverses south of Greenland, and continues along 60°N up to northern Scotland, as illustrated in Fig. 11a. Here, we analyze overturning from our model for years 11–15 and compare it to the longest time series of the OSNAP observations available to date (August 2014–May 2018; Lozier et al. 2019). Since our model and the observations cover different time periods, we do not expect to see exact correspondence between the two; nevertheless, a few things should be noted. The control run overestimates the strength of the overturning, particularly in the Labrador Sea (Fig. 10c), possibly due to larger salinities and larger densities in our model compared to observations (see section 3). It is common for higher-resolution models to overestimate the magnitude of overturning in subpolar latitudes (e.g., Petit et al. 2023). These models often feature a stronger subpolar gyre, leading to a greater impact of warm, saline subtropical Atlantic waters on the western subpolar gyre and resulting in greater dense water formation there, as discussed by Jackson et al. (2020).

Furthermore, our model does not demonstrate the same degree of density compensation as that inferred from the observations in the Labrador Sea (Zou et al. 2020) as in our case, the transformations in temperature and salinity space closely align with the values of overturning in density space across OSNAP West (not shown). The isopycnal of maximum overturning across OSNAP East is surprisingly consistent with the observations across all runs (Fig. 10b), even though all of our model runs have different thermohaline properties

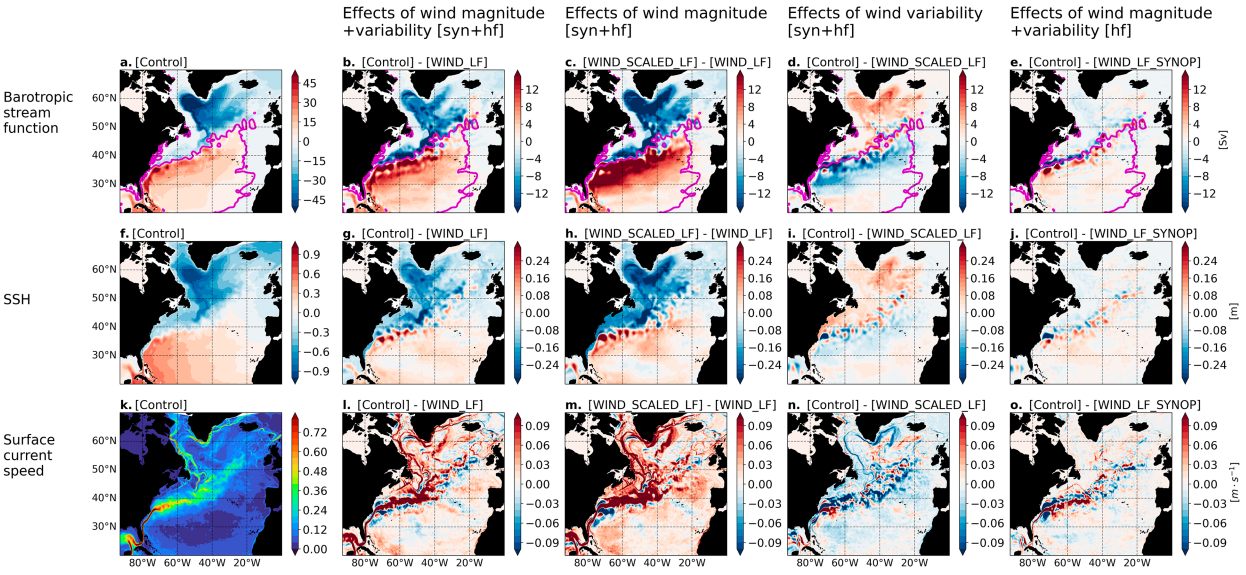

FIG. 7. (a) Barotropic streamfunction, (f) sea surface height, and (k) surface current speed, averaged over years 11–15 in control experiment. (b),(g),(l) The differences between control and experiment forced by low-frequency winds (highlighting the effect of wind magnitude and variability associated with synoptic and higher-frequency winds). (c),(h),(m) The differences between the experiments forced by scaled vs nonscaled low-frequency winds (highlighting the effect of wind magnitude associated with synoptic and higher-frequency winds). (d),(i),(n) The differences between control and experiment forced by scaled low-frequency winds (highlighting the effect of wind variability associated with synoptic and higher-frequency winds). (e),(j),(o) The differences between control and experiment forced by low-frequency and synoptic winds (highlighting the effect of wind magnitude and variability associated with synoptic and higher-frequency winds). Magenta contour lines in (a)–(e) show the zero line of the barotropic streamfunction in the control experiment, averaged over years 11–15.

in the eastern subpolar North Atlantic (Figs. 4 and 5). We also note that the WIND_LF experiment is the most consistent with observations in terms of the magnitude of the AMOC (Figs. 10a–c), despite the magnitude of the low-frequency wind forcing being weaker compared to the full atmospheric reanalysis winds and despite demonstrating too shallow mixed layer depths (Fig. 3g).

The variability in the overturning (shown in shading in Figs. 10a–c) is the lowest in the WIND_LF compared to all other experiments, including WIND_SCALED_LF. This suggests that a reduced magnitude of surface winds decreases overturning variability, while reduced high-frequency variability of surface winds without a change in magnitude does not have this effect. In all experiments, except for WIND_LF, overturning variability aligns with observations along OSNAP East and exceeds that along OSNAP West, while in the WIND_LF experiment, the opposite is true.

Surface water mass transformations have been computed following the methodology described in Walin (1982) and Tziperman (1986) for areas in the subpolar North Atlantic between 45°N and the northern boundary of our domain (Figs. 10d–f, regions north of the dashed white lines in Fig. 11a). These transformations show similar patterns to the overturning streamfunction (Figs. 10a–c); however, maximal values of water mass transformations correspond to lighter densities, which highlights the role of mixing that seems to be quite uniform in all model experiments. This is consistent with recent findings by Evans et al. (2023) who have shown that mixing plays an important role in setting the time-mean strength of the overturning streamfunction in the subpolar North Atlantic. The surface density in the WIND_LF experiment is generally lower than that in the other experiments and water mass transformations are shifted toward lighter densities compared to other experiments. To investigate whether the differences in surface water mass transformations are coming from differences in the surface densities or from differences in the air–sea fluxes, we also calculated surface water mass transformations using sea surface temperatures and salinities from the control run together with air–sea fluxes from each of the simulations with filtered winds (shown in dashed lines in Figs. 10d–f). The magnitudes of surface water mass transformation depend on the air–sea fluxes, while using different surface density fields allows us to match the densities of the maximal surface water mass transformation across all experiments.

Figure 11a shows the outcrops of isopycnals corresponding to the maximum AMOC in density space across the full OSNAP array in each of the experiments. All of these outcrops are very consistent in the eastern subpolar North Atlantic, while in the western part of the domain, the isopycnal of maximum overturning in the WIND_LF experiment outcrops only in the small region in the northern part of the Labrador Sea. This smaller area of the isopycnal outcrop could be the

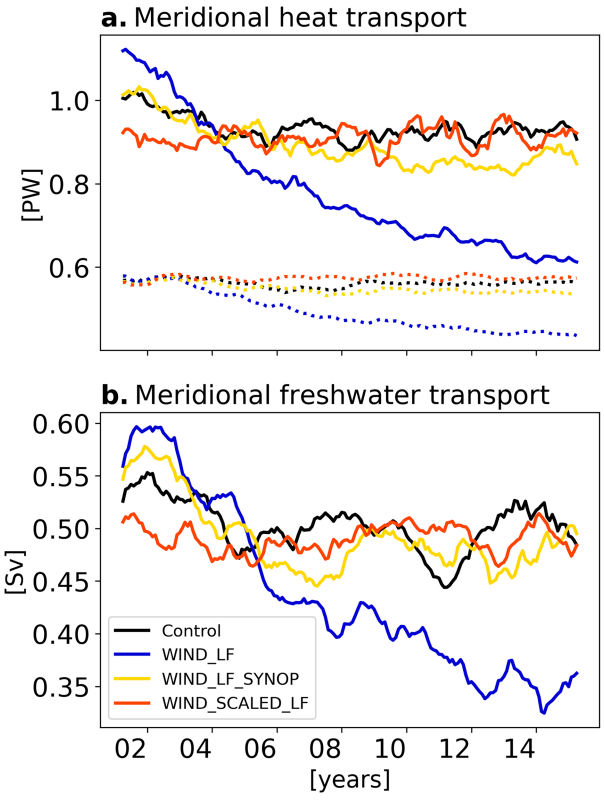

FIG. 8. Time series of (a) meridional heat and (b) freshwater transport across 40°N in control experiment (black) and sensitivity tests: experiment forced by low-frequency winds (blue), experiment forced by low-frequency + synoptic winds (yellow), and experiment forced by scaled low-frequency winds (red). Dotted lines in (a) show meridional heat transports across 60°N.

reason behind lower surface water mass transformations and overturning across the western part of the OSNAP array in the WIND_LF relative to the control run (Figs. 10c,f).

Figure 11b shows where the isopycnals corresponding to the maximum overturning along the OSNAP line outcrop at 63°N in the Labrador Sea (shown in cyan in Fig. 11a). Their structure is very consistent in all simulations; however, this outcrop encloses a much smaller area in the WIND_LF experiment. More generally, there is a strong relationship ($R^2 > 0.99$ for the mean values in four experiments) between the area of outcrop of the isopycnal corresponding to maximum overturning across a full OSNAP array in the western subpolar North Atlantic (north from 45°N and west from 45°W) and the strength of the overturning across the full OSNAP array. Density structure in the western subpolar North Atlantic defines the magnitude of overturning here: in Fig. 11c, using densities from WIND_LF and velocities from the control run in computing the overturning yields a similar overturning to the WIND_LF experiment, whereas using densities from the control experiment and velocities from the WIND_LF experiment results in a magnitude and shape of meridional overturning similar to the control run.

In the eastern subpolar North Atlantic, meridional transports are dominated by the East Greenland Current, and isopycnals of maximal overturning in each of the experiments are located at different depths in that region (Figs. 12a–d). Specifically, in the WIND_LF experiment, which differs the most from the control run, the isopycnal of maximal overturning is around 800 m deep, whereas it is closer to the surface in the control run. This suggests that the southward transport within the East Greenland Current (EGC) in the WIND_LF run is divided between upper and lower branches of the meridional overturning streamfunction (Fig. 12b), whereas in the control run, more of it is in the lower branch. Consequently, the variation of densities along this current plays a crucial role in determining the magnitude of overturning. This factor has also been acknowledged and discussed in the literature as a mechanism responsible for the seasonal variations of the overturning across OSNAP East (Wang et al. 2021; Tooth et al. 2023). Interestingly, the WIND_SCALED_LF experiment has a similar position of the isopycnal of maximal overturning compared to the control run (Fig. 12d) implying that high-frequency wind variability has a marginal effect on densities here, despite impacting the EGC transport.

Additionally, the boundary currents in the WIND_LF experiment are the weakest among all of our experiments (Fig. 12b, also see Fig. 7l). Therefore, in the eastern subpolar North Atlantic, the magnitude of overturning appears to be determined by both velocity and density structure. Figure 12e illustrates this by showing that combining densities from WIND_LF with velocities from the control run yields a similar density-space overturning as combining densities from the control run with velocities from the WIND_LF experiment, while both of these overturning streamfunctions lay between the control and WIND_LF experiments. In this way, winds impact the strength of the boundary currents and density structure in both the western and eastern subpolar North Atlantic. However, in the western subpolar North Atlantic, density changes seem to be more important for overturning, while in the eastern subpolar North Atlantic, the role of density is comparable with the changing strength of boundary currents.

6. Conclusions and discussion

In this paper, we have analyzed the response of the North Atlantic Ocean circulation to atmospheric dynamical processes on various time scales. For this purpose, we performed a suite of sensitivity experiments with a 1/12° regional configuration of the MITgcm where we applied low-pass filtering to surface winds to extract variability associated with subsynoptic (<2 days) and synoptic processes (2–10 days) in the atmosphere and examined the impact of wind magnitude and synoptic and subsynoptic variability on the circulation in the subpolar North Atlantic.

The magnitude of the surface winds seems to play a particularly important role for the western subpolar North Atlantic. In the first 5 years, we mostly observe the local effect of overall cooling due to the impact of winds on turbulent and latent heat fluxes and also on the mixing and an increase in the salinity in the Labrador Sea (Figs. 3b,g,l, and 5a). After 5 years,

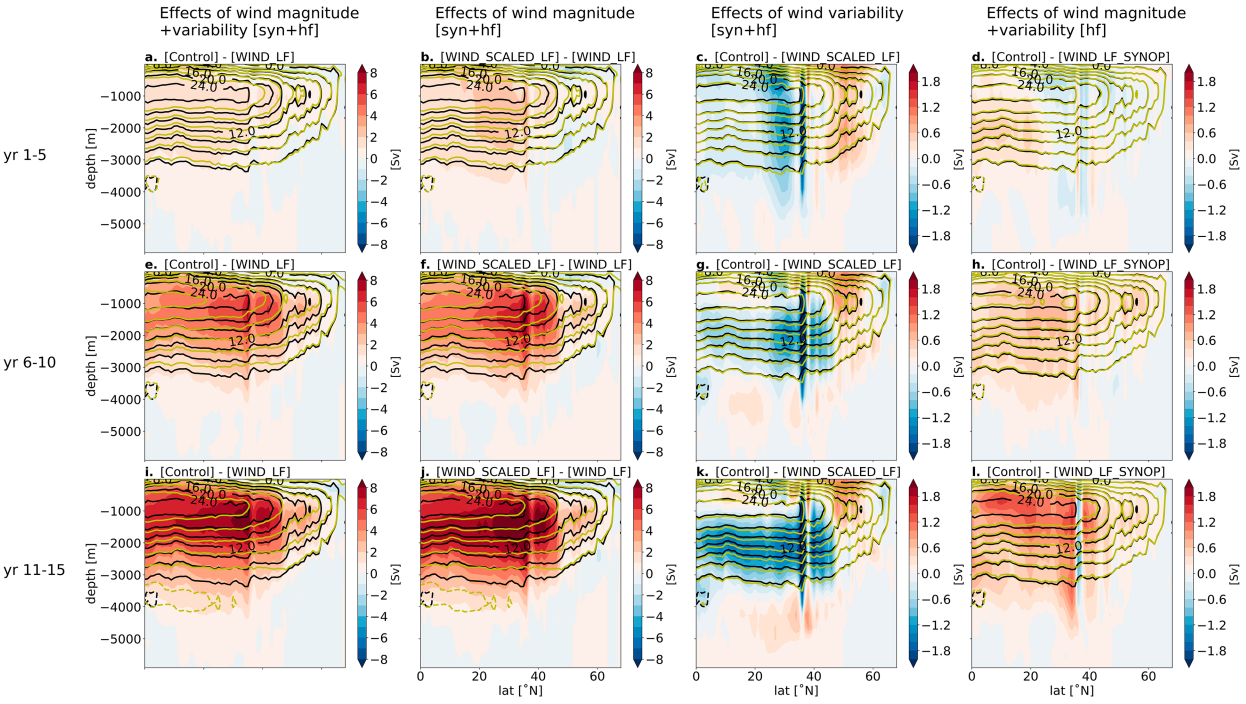

FIG. 9. Differences in meridional overturning streamfunction in depth space between the control run and sensitivity tests averaged over (a)–(d) years 1–5, (e)–(h) years 6–10, and (i)–(l) years 11–15; black contours show the meridional overturning streamfunction in the control run and yellow contours show that in each of the sensitivity experiments. (a),(e),(i) The differences between control and experiment forced by low-frequency winds (highlighting the effect of wind magnitude and variability associated with synoptic and higher-frequency winds). (b),(f),(j) The differences between the experiments forced by scaled vs nonscaled low-frequency winds (highlighting the effect of wind magnitude associated with synoptic and higher-frequency winds). (c),(g),(k) The differences between control and experiment forced by scaled low-frequency winds (highlighting the effect of wind variability associated with synoptic and higher-frequency winds). (d),(h),(l) The differences between control and experiment forced by low-frequency and synoptic winds (highlighting the effect of wind magnitude and variability associated with synoptic and higher-frequency winds). Note: The first two columns use different colormap limits compared to the third and fourth columns.

the advective feedbacks start to play a role: wind with larger magnitudes leads to a stronger subpolar gyre that in turn leads to stronger impact of the North Atlantic Current bringing warmer and saltier waters to the subpolar North Atlantic (Figs. 4 and 5a,e,i). Thus, both of these effects of the magnitude of surface winds associated with synoptic and higher-frequency atmospheric processes result in the densification of the upper waters in the western subpolar North Atlantic (Figs. 6a,e,i). This anomaly in the density of the upper ocean in the Labrador Sea, created by the effects of winds on both surface fluxes and ocean circulation, is important for the magnitude of overturning in the subpolar North Atlantic since it defines whether isopycnals corresponding to the maximum overturning will be in contact with the atmosphere and exposed to watermass transformation at the surface. This is consistent with a number of recent studies suggesting a strong relationship between overturning and salinity/density in the western subpolar North Atlantic (e.g., Hodson and Sutton 2012; Robson et al. 2016; Ortega et al. 2021; Jackson and Petit 2023). We also show that in the experiments with reduced winds, the magnitudes of surface water mass transformations are defined by the air–sea fluxes, while the density associated with maximal transformation depends on the surface density field (Figs. 10d–f). A reduced magnitude of surface winds in our experiment decreased interannual variability in overturning, while reduced high-frequency variability of surface winds did not have an effect on overturning variability (Figs. 10a–c).

After normalizing for the difference in wind energy input, we find that the variability of surface winds associated with synoptic and higher-frequency processes in the atmosphere reduces the heat loss in the Labrador Sea (Fig. 3d). The advection of the resulting warmer and saltier waters into the eastern subpolar gyre then leads to lower densities in the upper ocean there. Variability associated with synoptic and higher-frequency atmospheric processes also leads to weakening of the subpolar gyre and boundary currents due to the dampening effect of atmospheric eddies (Figs. 7d,n). The meridional overturning circulation in the eastern subpolar North Atlantic is sensitive to changes in the strength of the East Greenland Current and the depth of the isopycnal of maximum overturning there (Fig. 12). Such changes can alter the balance of southward flow in the upper and lower limbs, thus impacting the magnitude of overturning, which aligns with

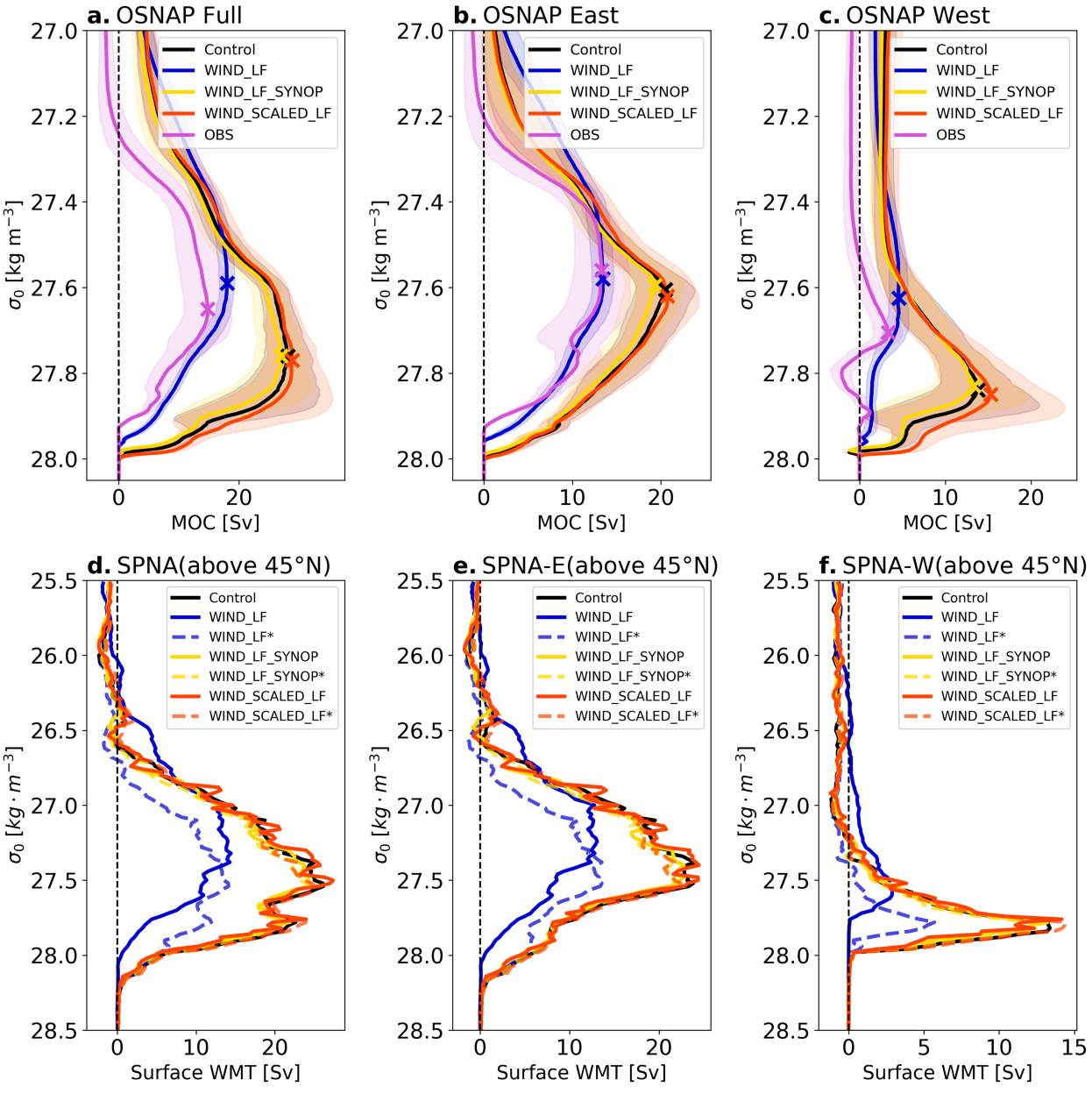

FIG. 10. (top) Meridional overturning streamfunction in density space across (a) the full OSNAP array, (b) OSNAP East, and (c) OSNAP West sections, from control experiment (black) and sensitivity tests (blue, yellow, and red) averaged over years 11–15 and compared to OSNAP observations (purple) averaged over August 2014–May 2018; standard deviation for each density class is shown in shading. The location of the OSNAP lines is illustrated in Fig. 11a. (bottom) Surface water mass transformations calculated within the region (d) north of 45°N, further separated into the regions (e) east of 45°W and (f) west of 45°W shown with the dashed lines in Fig. 11a.

evidence from previous studies (e.g., Wang et al. 2021; Tooth et al. 2023).

Surprisingly, despite the differences in thermohaline structure among the sensitivity tests, the overturning in density space in the eastern subpolar North Atlantic remains remarkably stable under different atmospheric forcings (Figs. 10a–c). The maximum overturning across OSNAP East occurs at very similar densities in all experiments. However, the experiments forced by winds with larger magnitudes exhibit stronger overturning, likely due to the strengthening of the subpolar gyre in these experiments. This observation is intriguing in light of recent findings by Fu et al. (2020) which indicate that the strength of the overturning in the subpolar North Atlantic has remained remarkably stable over the past few decades, despite changing thermohaline conditions. In our case, the strength of the AMOC in density space in

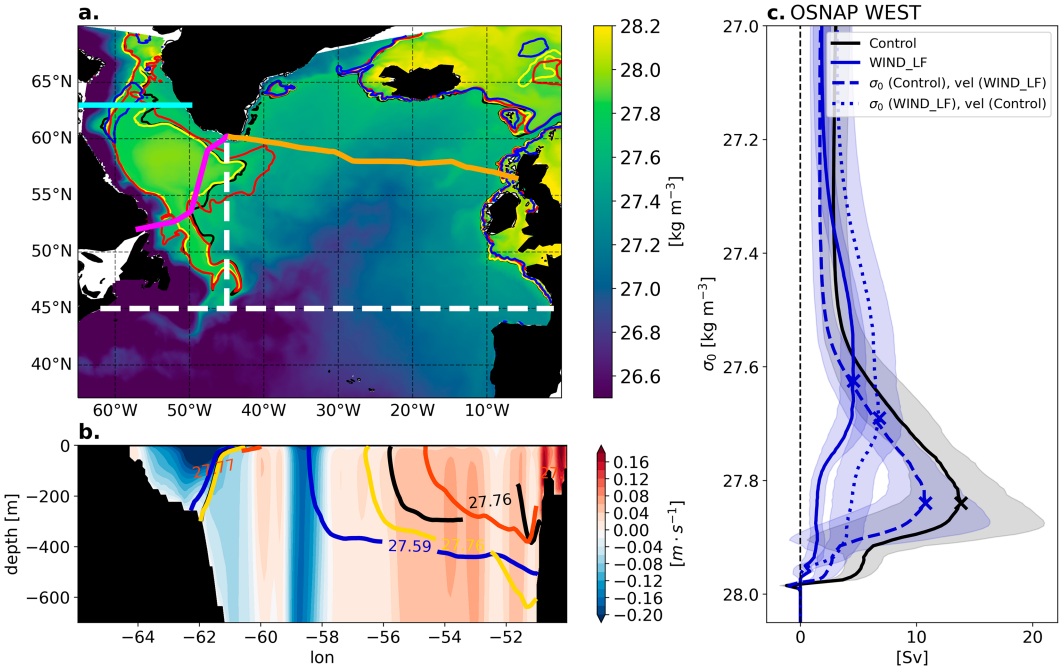

FIG. 11. (a) Mean surface potential density (σ_0) in winter (January–March) for the control experiment during years 11–15. Contour lines correspond to isopycnals of maximum overturning across OSNAP line (refer to Fig. 10) in the control experiment (black; σ_0 = 27.76 kg m^{-3}), WIND_LF (blue; σ_0 = 27.59 kg m^{-3}), WIND_LF_SYNOP (yellow; σ_0 = 27.76 kg m^{-3}), and WIND_SCALED_LF (red; σ_0 = 27.77 kg m^{-3}). Magenta and orange lines show the location of the observational OSNAP West and OSNAP East arrays, respectively; the regions used for calculating surface water mass transformations (shown in Figs. 10d–f) are positioned to the north of white dashed lines. (b) The mean velocity across the 63°N latitude in the Labrador Sea [shown in cyan line in (a)], with contour lines corresponding to the isopycnals of maximal overturning in our simulations across OSNAP line [color coding matches (a)]. (c) MOC in density space (MOCσ_0) across OSNAP West [purple line on (a)]: dashed blue line shows MOCσ_0 computed using densities from control experiment and velocities from WIND_LF; dotted blue line shows MOCσ_0 computed using densities from WIND_LF experiment and velocities from control experiment.

the eastern subpolar North Atlantic does vary across the different ocean states; however, the maximum overturning is consistently associated with the same isopycnals across all experiments, highlighting the robustness of this characteristic.

The subsynoptic (<2 days) variability of atmospheric winds has a marginal effect on the overturning in density space in the subpolar North Atlantic: the areas of isopycnal outcrop in the Labrador Sea and magnitude of overturning across OSNAP West exhibit only marginal differences from the control run (Figs. 10 and 11a). There is evidence in the literature that smaller-scale atmospheric features such as tip jets and cold-air outbreaks affect the water mass transformation particularly in the Irminger Sea (Våge et al. 2009; Condron and Renfrew 2013; Moore 2014; Papritz and Spengler 2017; Josey et al. 2019; Gutjahr et al. 2022). In our experiments, the effect of removing higher-frequency atmospheric variability seems to be similar to the effect of removing both synoptic and higher-frequency atmospheric processes, albeit with a lower magnitude of impact (Figs. 3 and 7–9). While marginally affecting the subpolar overturning in density space, the higher-frequency atmospheric variability generally makes the overturning in depth space stronger and leads to its core being slightly deeper, particularly in the subtropics (Figs. 9d,h,l).

Summarizing, we find the changes in the wind magnitude, and hence, the wind energy input in the region has the dominant effect on the strength of the overturning; once this is accounted for, the magnitude of the overturning in all sensitivity experiments is very similar to that of the control run. The major impacts from variability of surface winds associated with synoptic and subsynoptic processes on the AMOC arise from their impact on heat loss reduction in the Labrador Sea, alongside changes in the Ekman transports. This study highlights the importance of accurately representing the density structure in the Labrador Sea as well as both density structure and the strength of the East Greenland Current in models for the correct representation of overturning in the subpolar North Atlantic. These results also underscore the critical importance of continuous in situ observations in the Labrador Sea and along the boundary currents in the subpolar North Atlantic. This is crucial both to capture potential changes in the densities in the Irminger Sea due to Arctic freshwater influx and Greenland Ice Sheet melt in the present and future

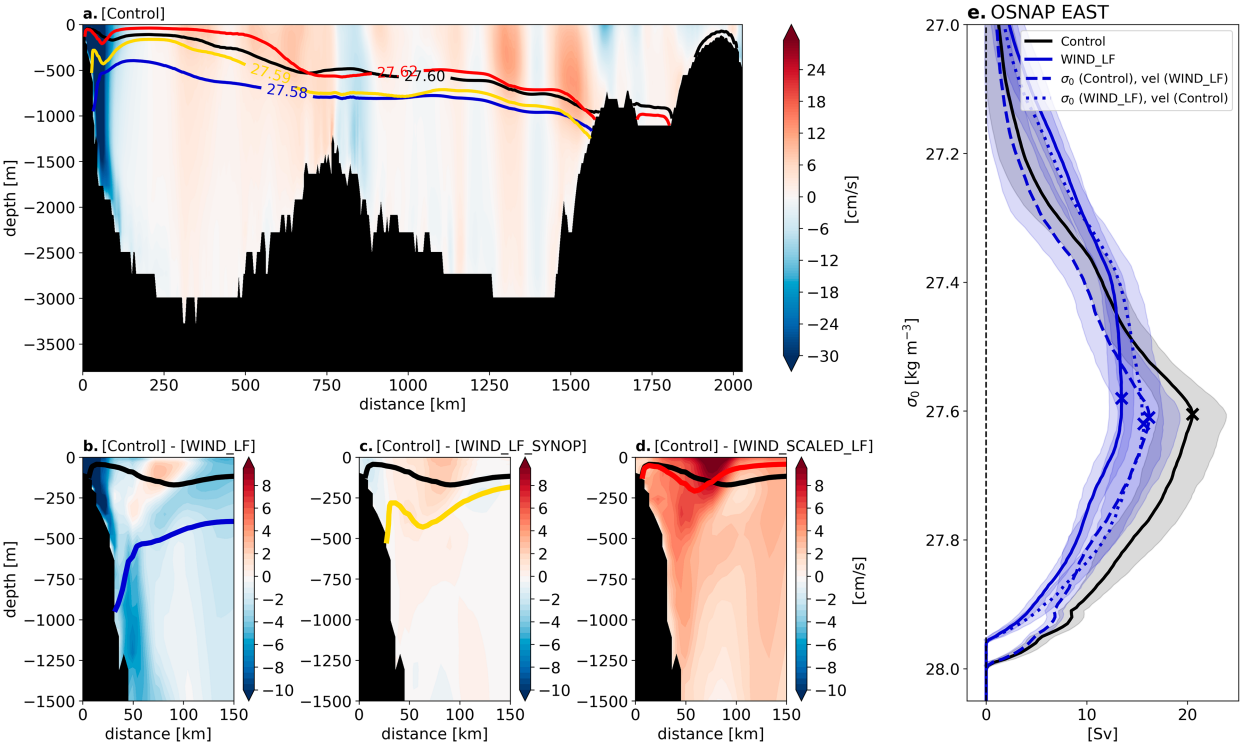

FIG. 12. (a) Mean velocity across the OSNAP East line (shown in Fig. 11 with solid orange line) in the control experiment; contours show annual mean positions of isopycnals of maximal overturning across OSNAP East in the control experiment (black), WIND_LF (blue), WIND_LF_SYNOP (yellow), and WIND_SCALED_LF (red). (b) Differences between control and experiment forced by low-frequency winds. (c) The differences between control and experiment forced by low-frequency and synoptic winds. (d) The differences between control and experiment forced by scaled low-frequency winds. (e) MOCσ_0 across OSNAP East (purple line in Fig. 11a): dashed blue line shows MOCσ_0 computed using densities from control experiment and velocities from WIND_LF; dotted blue line shows MOCσ_0 computed using densities from WIND_LF experiment and velocities from control experiment.

climate, and, in turn, their impacts on the strength of the gyre and overturning circulation.

Acknowledgments. The numerical simulations were performed using the ARCHER2 U.K. National Supercomputing Service (https://www.archer2.ac.uk) and JASMIN, the U.K. collaborative data analysis facility. M. Y. M., H. L. J., and D. P. M. were funded by the U.K. National Environmental Research Council through the SNAP-DRAGON project (NE/T013494/1). We thank An Nguyen and Patrick Heimbach for their help with setting up the model, as well as Oliver Tooth and the SNAP-DRAGON community for useful discussions. We are grateful to Nicholas Foukal and an anonymous reviewer for constructive comments and suggestions that helped to improve the manuscript.

Data availability statement. All data produced and analyzed in this study can be found at https://catalogue.ceda.ac.uk/uuid/8c1bd495fc7c442ba0d62b8830f716cf (Markina et al. 2024a) and https://catalogue.ceda.ac.uk/uuid/9536459d09fb446d8daee987a039616e (Markina et al. 2024b). The MITgcm source code is available online at mitgcm.org. OSNAP data are available at https://www.o-snap.org/.

REFERENCES

Adcroft, A., and J.-M. Campin, 2004: Rescaled height coordinates for accurate representation of free-surface flows in ocean circulation models. *Ocean Modell.*, **7**, 269–284, https://doi.org/10.1016/j.ocemod.2003.09.003.

——, and Coauthors, 2018: MITgcm user manual. 485 pp., http://hdl.handle.net/1721.1/117188.

Ayrault, F., F. Lalaurette, A. Joly, and C. Loo, 1995: North Atlantic ultra high frequency variability: An introductory survey. *Tellus*, **47A**, 671–696, https://doi.org/10.3402/tellusa.v47i5.11565.

Barnier, B., 1988: A numerical study on the influence of the mid-Atlantic ridge on nonlinear 1st-mode baroclinic Rossby waves generated by seasonal winds. *J. Phys. Oceanogr.*, **18**, 417–433, https://doi.org/10.1175/1520-0485(1988)018<0417:ANSOTI>2.0.CO;2.

Barrier, N., C. Cassou, J. Deshayes, and A.-M. Treguier, 2014: Response of North Atlantic Ocean circulation to atmospheric weather regimes. *J. Phys. Oceanogr.*, **44**, 179–201, https://doi.org/10.1175/JPO-D-12-0217.1.

Biastoch, A., C. W. Böning, J. Getzlaff, J.-M. Molines, and G. Madec, 2008: Causes of interannual–decadal variability in the meridional overturning circulation of the midlatitude North Atlantic Ocean. *J. Climate*, **21**, 6599–6615, https://doi.org/10.1175/2008JCLI2404.1.

Böning, C. W., M. Scheinert, J. Dengg, A. Biastoch, and A. Funk, 2006: Decadal variability of subpolar gyre transport and its reverberation in the North Atlantic overturning. *Geophys. Res. Lett.*, **33**, L21S01, https://doi.org/10.1029/2006GL026906.

Buckley, M. W., and J. Marshall, 2016: Observations, inferences, and mechanisms of the Atlantic meridional overturning circulation: A review. *Rev. Geophys.*, **54**, 5–63, https://doi.org/10.1002/2015RG000493.

Chafik, L., N. P. Holliday, S. Bacon, and T. Rossby, 2022: Irminger Sea is the center of action for subpolar AMOC variability. *Geophys. Res. Lett.*, **49**, e2022GL099133, https://doi.org/10.1029/2022GL099133.

Chassignet, E. P., and D. P. Marshall, 2008: Gulf stream separation in numerical ocean models. *Ocean Modeling in an Eddying Regime*, *Geophys. Monogr.*, Vol. 177, Amer. Geophys. Union, 39–61, https://doi.org/10.1029/177GM05.

Condron, A., and I. A. Renfrew, 2013: The impact of polar mesoscale storms on northeast Atlantic Ocean circulation. *Nat. Geosci.*, **6**, 34–37, https://doi.org/10.1038/ngeo1661.

Danabasoglu, G., and Coauthors, 2016: North Atlantic simulations in Coordinated Ocean-ice Reference Experiments phase II (CORE-II). Part II: Inter-annual to decadal variability. *Ocean Modell.*, **97**, 65–90, https://doi.org/10.1016/j.ocemod.2015.11.007.

Delworth, T. L., and R. J. Greatbatch, 2000: Multidecadal thermohaline circulation variability driven by atmospheric surface flux forcing. *J. Climate*, **13**, 1481–1495, https://doi.org/10.1175/1520-0442(2000)013<1481:MTCVDB>2.0.CO;2.

Deshayes, J., and C. Frankignoul, 2008: Simulated variability of the circulation in the North Atlantic from 1953 to 2003. *J. Climate*, **21**, 4919–4933, https://doi.org/10.1175/2008JCLI1882.1.

Duchon, C. E., 1979: Lanczos filtering in one and two dimensions. *J. Appl. Meteor.*, **18**, 1016–1022, https://doi.org/10.1175/1520-0450(1979)018<1016:LFIOAT>2.0.CO;2.

Eden, C., and T. Jung, 2001: North Atlantic interdecadal variability: Oceanic response to the North Atlantic Oscillation (1865–1997). *J. Climate*, **14**, 676–691, https://doi.org/10.1175/1520-0442(2001)014<0676:NAIVOR>2.0.CO;2.

——, and J. Willebrand, 2001: Mechanism of interannual to decadal variability of the North Atlantic circulation. *J. Climate*, **14**, 2266–2280, https://doi.org/10.1175/1520-0442(2001)014<2266:MOITDV>2.0.CO;2.

Evans, D. G., N. P. Holliday, S. Bacon, and I. Le Bras, 2023: Mixing and air–sea buoyancy fluxes set the time-mean overturning circulation in the subpolar North Atlantic and Nordic Seas. *Ocean Sci.*, **19**, 745–768, https://doi.org/10.5194/os-19-745-2023.

Foussard, A., G. Lapeyre, and R. Plougonven, 2019: Storm tracks response to oceanic eddies in idealized atmospheric simulations. *J. Climate*, **32**, 445–463, https://doi.org/10.1175/JCLI-D-18-0415.1.

Fox, A. D., and Coauthors, 2022: Exceptional freshening and cooling in the eastern subpolar North Atlantic caused by reduced Labrador Sea surface heat loss. *Ocean Sci.*, **18**, 1507–1533, https://doi.org/10.5194/os-18-1507-2022.

Fu, Y., F. Li, J. Karstensen, and C. Wang, 2020: A stable Atlantic Meridional overturning circulation in a changing North Atlantic Ocean since the 1990s. *Sci. Adv.*, **6**, eabc7836, https://doi.org/10.1126/sciadv.abc7836.

Furey, H. H., N. P. Foukal, A. Anderson, and A. S. Bower, 2023: Investigation of the source of Iceland basin freshening: Virtual particle tracking with satellite-derived geostrophic surface velocities. *Remote Sens.*, **15**, 5711, https://doi.org/10.3390/rs15245711.

Gulev, S., T. Jung, and E. Ruprecht, 2002: Climatology and interannual variability in the intensity of synoptic-scale processes in the North Atlantic from the NCEP–NCAR reanalysis data. *J. Climate*, **15**, 809–828, https://doi.org/10.1175/1520-0442(2002)015%3C0809:CAIVIT%3E2.0.CO;2.

Gutjahr, O., J. H. Jungclaus, N. Brüggemann, H. Haak, and J. Marotzke, 2022: Air-sea interactions and water mass transformation during a katabatic storm in the Irminger Sea. *J. Geophys. Res. Oceans*, **127**, e2021JC018075, https://doi.org/10.1029/2021JC018075.

Heimbach, P., D. Menemenlis, M. Losch, J.-M. Campin, and C. Hill, 2010: On the formulation of sea-ice models. Part 2: Lessons from multi-year adjoint sea-ice export sensitivities through the Canadian Arctic Archipelago. *Ocean Modell.*, **33**, 145–158, https://doi.org/10.1016/j.ocemod.2010.02.002.

Hirschi, J.-M., and Coauthors, 2020: The Atlantic meridional overturning circulation in high resolution models. *J. Geophys. Res. Oceans*, **125**, e2019JC015522, https://doi.org/10.1029/2019JC015522.

Hodson, D. L. R., and R. T. Sutton, 2012: The impact of resolution on the adjustment and decadal variability of the Atlantic meridional overturning circulation in a coupled climate model. *Climate Dyn.*, **39**, 3057–3073, https://doi.org/10.1007/s00382-012-1309-0.

Holliday, N. P., and Coauthors, 2020: Ocean circulation causes the largest freshening event for 120 years in eastern subpolar North Atlantic. *Nat. Commun.*, **11**, 585, https://doi.org/10.1038/s41467-020-14474-y.

Holte, J., L. D. Talley, J. Gilson, and D. Roemmich, 2017: An Argo mixed layer climatology and database. *Geophys. Res. Lett.*, **44**, 5618–5626, https://doi.org/10.1002/2017GL073426.

Hoskins, B. J., and K. I. Hodges, 2002: New perspectives on the Northern Hemisphere winter storm tracks. *J. Atmos. Sci.*, **59**, 1041–1061, https://doi.org/10.1175/1520-0469(2002)059<1041:NPOTNH>2.0.CO;2.

IPCC, 2021: *Climate Change 2021: The Physical Science Basis*. V. Masson-Delmotte et al., Eds., Cambridge University Press, 2391 pp., https://doi.org/10.1017/9781009157896.

Jackson, L. C., and T. Petit, 2023: North Atlantic overturning and water mass transformation in CMIP6 models. *Climate Dyn.*, **60**, 2871–2891, https://doi.org/10.1007/s00382-022-06448-1.

——, and Coauthors, 2020: Impact of ocean resolution and mean state on the rate of AMOC weakening. *Climate Dyn.*, **55**, 1711–1732, https://doi.org/10.1007/s00382-020-05345-9.

——, A. Biastoch, M. W. Buckley, D. G. Desbruyères, E. Frajka-Williams, B. Moat, and J. Robson, 2022: The evolution of the North Atlantic meridional overturning circulation since 1980. *Nat. Rev. Earth Environ.*, **3**, 241–254, https://doi.org/10.1038/s43017-022-00263-2.

Josey, S. A., M. F. de Jong, M. Oltmanns, G. K. Moore, and R. A. Weller, 2019: Extreme variability in Irminger Sea winter heat loss revealed by ocean observatories initiative mooring and the ERA5 reanalysis. *Geophys. Res. Lett.*, **46**, 293–302, https://doi.org/10.1029/2018GL080956.

Khatri, H., R. G. Williams, T. Woollings, and D. M. Smith, 2022: Fast and slow subpolar ocean responses to the North Atlantic Oscillation: Thermal and dynamical changes. *Geophys. Res. Lett.*, **49**, e2022GL101480, https://doi.org/10.1029/2022GL101480.

Kostov, Y., and Coauthors, 2021: Distinct sources of interannual subtropical and subpolar Atlantic overturning variability. *Nat. Geosci.*, **14**, 491–495, https://doi.org/10.1038/s41561-021-00759-4.

Lanczos, C., 1956: *Applied Analysis*. Prentice-Hall, 539 pp.

Larson, S. M., M. W. Buckley, and A. C. Clement, 2020: Extracting the buoyancy-driven Atlantic meridional overturning circulation. *J. Climate*, **33**, 4697–4714, https://doi.org/10.1175/JCLI-D-19-0590.1.

Li, F., and Coauthors, 2021: Subpolar North Atlantic western boundary density anomalies and the meridional overturning circulation. *Nat. Commun.*, **12**, 3002, https://doi.org/10.1038/s41467-021-23350-2.

Lohmann, K., H. Drange, and M. Bentsen, 2009: Response of the North Atlantic subpolar gyre to persistent North Atlantic Oscillation like forcing. *Climate Dyn.*, **32**, 273–285, https://doi.org/10.1007/s00382-008-0467-6.

——, D. A. Putrasahan, J.-S. von Storch, O. Gutjahr, J. H. Jungclaus, and H. Haak, 2021: Response of northern North Atlantic and Atlantic meridional overturning circulation to reduced and enhanced wind stress forcing. *J. Geophys. Res. Oceans*, **126**, e2021JC017902, https://doi.org/10.1029/2021JC017902.

Losch, M., D. Menemenlis, J.-M. Campin, P. Heimbach, and C. Hill, 2010: On the formulation of sea-ice models. Part 1: Effects of different solver implementations and parameterizations. *Ocean Modell.*, **33**, 129–144, https://doi.org/10.1016/j.ocemod.2009.12.008.

Lozier, M. S., and Coauthors, 2019: A sea change in our view of overturning in the subpolar North Atlantic. *Science*, **363**, 516–521, https://doi.org/10.1126/science.aau6592.

Markina, M. Y., J. H. P. Studholme, and S. K. Gulev, 2019: Ocean wind wave climate responses to wintertime North Atlantic atmospheric transient eddies and low-frequency flow. *J. Climate*, **32**, 5619–5638, https://doi.org/10.1175/JCLI-D-18-0595.1.

——, H. L. Johnson, and D. P. Marshall, 2024a: Control run of a 1/12° regional simulation of MITgcm in the North Atlantic Ocean (repeated year forcing from JRA55-do, May 2003–May 2004. NERC EDS British Oceanographic Data Centre NOC, accessed 12 January 2024, https://doi.org/10.5285/0e1fef66-1ab4-3002-e063-6c86abc0d49a.

——, ——, and ——, 2024b: Sensitivity experiments with a 1/12° regional configuration of MITgcm in the North Atlantic Ocean (repeated year forcing from JRA55-do, May 2003–May 2004) with forced surface winds extracting variability in subsynoptic and synoptic processes. NERC EDS British Oceanographic Data Centre NOC, accessed 12 January 2024, https://doi.org/10.5285/0e1fee70-94fd-2f71-e063-6c86abc0a403.

Marshall, J., A. Adcroft, C. Hill, L. Perelman, and C. Heisey, 1997: A finite-volume, incompressible Navier Stokes model for studies of the ocean on parallel computers. *J. Geophys. Res.*, **102**, 5753–5766, https://doi.org/10.1029/96JC02775.

——, H. Johnson, and J. Goodman, 2001: A study of the interaction of the North Atlantic oscillation with ocean circulation. *J. Climate*, **14**, 1399–1421, https://doi.org/10.1175/1520-0442(2001)014<1399:ASOTIO>2.0.CO;2.

Martin, T., A. Reintges, and M. Latif, 2019: Coupled North Atlantic subdecadal variability in CMIP5 models. *J. Geophys. Res. Oceans*, **124**, 2404–2417, https://doi.org/10.1029/2018JC014539.

Menary, M. B., D. L. R. Hodson, J. I. Robson, R. T. Sutton, R. A. Wood, and J. A. Hunt, 2015: Exploring the impact of CMIP5 model biases on the simulation of North Atlantic decadal variability. *Geophys. Res. Lett.*, **42**, 5926–5934, https://doi.org/10.1002/2015GL064360.

Moat, B. I., and Coauthors, 2020: Pending recovery in the strength of the meridional overturning circulation at 26° N. *Ocean Sci.*, **16**, 863–874, https://doi.org/10.5194/os-16-863-2020.

Moore, G. W. K., 2014: Mesoscale structure of Cape Farewell tip jets. *J. Climate*, **27**, 8956–8965, https://doi.org/10.1175/JCLI-D-14-00299.1.

Nguyen, A. T., H. Pillar, V. Ocaña, A. Bigdeli, T. A. Smith, and P. Heimbach, 2021: The Arctic subpolar gyre sTate estimate: Description and assessment of a data-constrained, dynamically consistent ocean-sea ice estimate for 2002–2017. *J. Adv. Model. Earth Syst.*, **13**, e2020MS002398, https://doi.org/10.1029/2020MS002398.

Ortega, P., and Coauthors, 2021: Labrador Sea subsurface density as a precursor of multidecadal variability in the North Atlantic: A multi-model study. *Earth Syst. Dyn.*, **12**, 419–438, https://doi.org/10.5194/esd-12-419-2021.

Papritz, L., and T. Spengler, 2017: A Lagrangian climatology of wintertime cold air outbreaks in the Irminger and Nordic Seas and their role in shaping air–sea heat fluxes. *J. Climate*, **30**, 2717–2737, https://doi.org/10.1175/JCLI-D-16-0605.1.

Petit, T., J. Robson, D. Ferreira, and L. C. Jackson, 2023: Understanding the sensitivity of the North Atlantic subpolar overturning in different resolution versions of HadGEM3-GC3.1. *J. Geophys. Res. Oceans*, **128**, e2023JC019672, https://doi.org/10.1029/2023JC019672.

Priestley, M. D. K., D. Ackerley, J. L. Catto, K. I. Hodges, R. E. McDonald, and R. W. Lee, 2020: An overview of the extratropical storm tracks in CMIP6 historical simulations. *J. Climate*, **33**, 6315–6343, https://doi.org/10.1175/JCLI-D-19-0928.1.

——, ——, ——, and ——, 2023: Drivers of biases in the CMIP6 extratropical storm tracks. Part I: Northern Hemisphere. *J. Climate*, **36**, 1451–1467, https://doi.org/10.1175/JCLI-D-20-0976.1.

Putrasahan, D. A., K. Lohmann, J.-S. von Storch, J. H. Jungclaus, O. Gutjahr, and H. Haak, 2019: Surface flux drivers for the slowdown of the Atlantic Meridional Overturning Circulation in a high-resolution global coupled climate model. *J. Adv. Model. Earth Syst.*, **11**, 1349–1363, https://doi.org/10.1029/2018MS001447.

Robson, J., P. Ortega, and R. Sutton, 2016: A reversal of climatic trends in the North Atlantic since 2005. *Nat. Geosci.*, **9**, 513–517, https://doi.org/10.1038/ngeo2727.

Sarafanov, A., 2009: On the effect of the North Atlantic Oscillation on temperature and salinity of the subpolar North Atlantic intermediate and deep waters. *ICES J. Mar. Sci.*, **66**, 1448–1454, https://doi.org/10.1093/icesjms/fsp094.

Sinha, B., B. Topliss, A. T. Blaker, and J.-M. Hirschi, 2013: A numerical model study of the effects of interannual time scale wave propagation on the predictability of the Atlantic meridional overturning circulation. *J. Geophys. Res. Oceans*, **118**, 131–146, https://doi.org/10.1029/2012JC008334.

Stewart, K. D., and Coauthors, 2020: JRA55-do-based repeat year forcing datasets for driving ocean–sea-ice models. *Ocean Modell.*, **147**, 101557, https://doi.org/10.1016/j.ocemod.2019.101557.

Tooth, O. J., H. L. Johnson, C. Wilson, and D. G. Evans, 2023: Seasonal overturning variability in the eastern North Atlantic subpolar gyre: A Lagrangian perspective. *Ocean Sci.*, **19**, 769–791, https://doi.org/10.5194/os-19-769-2023.

Tsujino, H., and Coauthors, 2018: JRA-55 based surface dataset for driving ocean–sea-ice models (JRA55-do). *Ocean Modell.*, **130**, 79–139, https://doi.org/10.1016/j.ocemod.2018.07.002.

Tziperman, E., 1986: On the role of interior mixing and air-sea fluxes in determining the stratification and circulation of the oceans. *J. Phys. Oceanogr.*, **16**, 680–693, https://doi.org/10.1175/1520-0485(1986)016<0680:OTROIM>2.0.CO;2.

Våge, K., T. Spengler, H. C. Davies, and R. S. Pickart, 2009: Multi-event analysis of the westerly Greenland tip jet based upon 45 winters in ERA-40. *Quart. J. Roy. Meteor. Soc.*, **135**, 1999–2011, https://doi.org/10.1002/qj.488.

Visbeck, M., H. Cullen, G. Krahmann, and N. Naik, 1998: An ocean model's response to North Atlantic Oscillation-like wind forcing. *Geophys. Res. Lett.*, **25**, 4521–4524, https://doi.org/10.1029/1998GL900162.

Walin, G., 1982: On the relation between sea-surface heat flow and thermal circulation in the ocean. *Tellus*, **34**, 187–195, https://doi.org/10.3402/tellusa.v34i2.10801.

Wang, H., J. Zhao, F. Li, and X. Lin, 2021: Seasonal and interannual variability of the meridional overturning circulation in the subpolar North Atlantic diagnosed from a high resolution reanalysis data set. *J. Geophys. Res. Oceans*, **126**, e2020JC017130, https://doi.org/10.1029/2020JC017130.

Xu, X., H. E. Hurlburt, W. J. Schmitz Jr., R. Zantopp, J. Fischer, and P. J. Hogan, 2013: On the currents and transports connected with the Atlantic meridional overturning circulation in the subpolar North Atlantic. *J. Geophys. Res. Oceans*, **118**, 502–516, https://doi.org/10.1002/jgrc.20065.

Yang, H., K. Wang, H. Dai, Y. Wang, and Q. Li, 2016: Wind effect on the Atlantic meridional overturning circulation via sea ice and vertical diffusion. *Climate Dyn.*, **46**, 3387–3403, https://doi.org/10.1007/s00382-015-2774-z.

Yeager, S., and G. Danabasoglu, 2014: The origins of late twentieth-century variations in the large-scale North Atlantic circulation. *J. Climate*, **27**, 3222–3247, https://doi.org/10.1175/JCLI-D-13-00125.1.

Zou, S., M. Susan Lozier, F. Li, R. Abernathey, and L. Jackson, 2020: Density-compensated overturning in the Labrador Sea. *Nat. Geosci.*, **13**, 121–126, https://doi.org/10.1038/s41561-019-0517-1.